

Article

Study on Transient Overvoltage of Offshore Wind Farm Considering Different Electrical Characteristics of Vacuum Circuit Breaker

Zikai Zhou ^{1,†} , Yaxun Guo ^{1,†} , Xiaofeng Jiang ² , Gang Liu ^{1,*} , Wenhui Tang ^{1,*} ,
Honglei Deng ¹, Xiaohua Li ¹ and Ming Zheng ³

¹ School of Electric Power Engineering, South China University of Technology, Guangzhou 510640, China

² Jieyang Power Supply Bureau of Guangdong Power Grid Co., Ltd., Jieyang 522000, China

³ China Energy Engineering Group Guangdong Electric Power Design Institute Co., Ltd., Guangzhou 510663, China

* Correspondence: liugang@scut.edu.cn (G.L.); wenhutang@scut.edu.cn (W.T.); Tel.: +86-20-87110613 (G.L.); +86-20-87111422 (W.T.)

† These authors contributed equally to this work.

Received: 9 October 2019; Accepted: 29 October 2019; Published: 13 November 2019



Abstract: For the study of transient overvoltage (TOV) in an offshore wind farm (OWF) collector system caused by switching off vacuum circuit breakers (VCBs), a simplified experimental platform of OWF medium-voltage (MV) cable collector system was established in this paper to conduct switching operation tests of VCB and obtain the characteristic parameters for VCB, especially dielectric strength parameters; also, the effectiveness of the VCB reignition model was verified. Then, PSCAD/EMTDC was used to construct the MV collector system of the OWF, and the effects of normal switching and fault switching on TOV amplitude, steepness, and the total number of reignition of the VCB were studied, respectively, with the experimental parameters and traditional parameters of dielectric strength of the VCB. The simulation results show that when the VCB is at the tower bottom, the overvoltage amplitude generated by the normal switching is the largest, which is 1.83 p.u., and the overvoltage steepness of the fault switching is the largest, up to 142 kV/ μ s. The overvoltage amplitude and steepness caused by switching off VCB at the tower bottom faultily with traditional parameters are about 2 and 1.5 times of the experimental parameters under the same operating condition.

Keywords: offshore wind farm; vacuum circuit breaker; reignition characteristics; switching overvoltage

1. Introduction

Large wind farms are moving from land to sea to provide a richer and more stable source of clean energy [1,2]. Being increasingly valued by countries around the world, the operation and maintenance of offshore wind farms (OWFs) have been paid more and more attention [3,4]. Large-scale OWFs use cables as the collector system. Thus, the loads of the cables cannot exceed the limit of the cable ampacity [5,6], and the cables should be insulated reliably [7,8]. Moreover, the safety of the tower terminal transformers needs to be carefully considered. In 2004, at Horns Rev, the largest OWF in Denmark at that time, almost all the tower terminal transformers suffered insulation fault accidents [9]. In [10], the authors reported an accident of transformer insulation damage occurred by switching off a vacuum circuit breaker (VCB) after connecting with the shunt reactor in Wailuo OWF. Studies have shown that the high-frequency (HF) overvoltage generated by the frequent switching on and off for VCBs was the main factor causing insulation fault of the transformers [11–13]. Lars Lijstrand et al. simulated and calculated the HF transient process of operating overvoltage generated by switching on a no-load transformer and switching off a no-load transformer under a

single-phase grounding short-circuit fault in a medium-voltage (MV) collection grid of OWF [14]. Xuezhong Liu et al. established a test circuit for the MV cable simulation system of the wind farm and a simulation calculation platform of power-frequency overvoltage [15]. Combined with the simulation and field measurement data, the influence of VCB parameters and cable length on the transient overvoltage (TOV) generated by switching off the no-load transformer in the MV collector system of OWF was studied in [16]. PSCAD/EMTDC (Manitoba HVDC Research Centre, a division of MHI Ltd., Winnipeg, Canada) and DIgSILENT/PowerFactory (DIgSILENT GmbH, Gomaringen, Germany) were used to carry out simulation calculation of switching overvoltage when the operating feeder of the OWF was a long no-load cable, and it was compared with the measured data of the actual OWF in [17]. Although there have been a lot of studies on TOV of OWFs, they mainly focus on the qualitative analysis of amplitude and steepness of the switching on TOV in the power collector system. However, there is limited literature on the study of switching-off overvoltage in a power collector system and the quantitative analysis of the overvoltage steepness. Furthermore, with the improvement of manufacturing for VCBs, the traditional electrical parameters have not adapted to today’s research.

This paper mainly introduces a reignition modelling method and model verification of VCB in the OWF collector system, and also studies the characteristics of switching TOV in an OWF collector system, respectively, with the experimental parameters and traditional parameters of the dielectric strength of VCB.

The structure of this article is as follows. In Section 2, the models of double-fed induction generator (DFIG) and the VCB are established. In Section 3, the switching reignition experiment of VCB is conducted on the established experimental platform. The characteristic parameters of VCB are obtained, and the validity of the model is verified. Section 4 introduces the switching mode of the internal electrical system in OWF. In Section 5, a single-feeder MV cable collector system of OWF is constructed. The traditional parameters and experimental parameters are, respectively, used for the dielectric strength of the VCB model. The effects of normal switching and fault switching on TOV amplitude, steepness, and the total number of reignition at the high voltage side of the terminal transformer are compared. Finally, conclusions are drawn in Section 6.

2. System Component Simulation Model

2.1. DFIG Model

DFIGs are widely used in OWFs. The simplified DFIG model is composed of a wound induction motor, wind turbine components, double-pulse width modulation (PWM) converter, control system components, and filters both on the stator side and rotor side of the motor [18,19], as shown in Figure 1. The stray capacitances generally include the capacitances between stator winding and shell, stator winding and rotor, and rotor and shell. However, as the capacitance of the HF filter in the wind turbine is much larger than the capacitances mentioned above, stray capacitance has little influence on overvoltage. The study is conducted on the high-voltage side of the terminal transformer, so the stray capacitance of the induction motor can be ignored [20]. In this paper, the rated capacity of the DFIG is 4 MW.

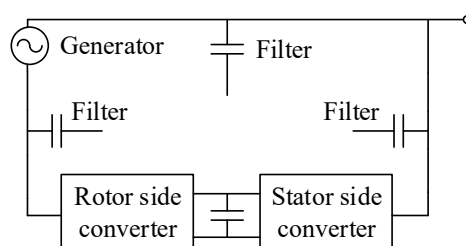


Figure 1. The double-fed induction generator (DFIG) model.

2.2. VCB Model

For inductive circuits, after the current is cut off near the zero-crossing point, an overvoltage will be caused by current chopping, which may result in the first reignition. During reignition, HF current is generated due to the influence of circuit parameters. When the HF current is cut off, the equivalent capacitance and inductance on the load side will cause electromagnetic oscillation. This oscillation will result in higher voltage that may cause the contact gap to be broken down again. Also, the HF current may couple to the other phases, producing current zeros. Thus virtual chopping occurs, causing overvoltage in other phases [10,21]. In the process of multiple reignitions, the interval between the two reignitions is extremely short. Since the second reignition is based on the previous reignition, the reignition overvoltage has the characteristics of high steepness and high amplitude,

The actual parameters of VCB are statistical and random. However, in order to study the switching overvoltage of the VCB, the parameters are set as constant values in this paper [22].

2.2.1. Chopping Current

When a VCB receives an opening instruction, the power frequency current is suddenly cut off before it reaches zero for the first time. The value of current at this time is called chopping current. When the load current varies in the range of 10 A–100 kA, the calculation for chopping current I_{ch} of VCB is as the following empirical formula:

$$I_{ch} = (2\pi I f \alpha \beta)^{\frac{1}{1-\beta}}, \quad (1)$$

where f is power frequency (s^{-1}); I is current amplitude before cut-off in the first half cycle (A); and α and β are related to electrode size, material, gap distance, and circuit parameters, where $\alpha = 6.2 \times 10^{-16}$ s, $\beta = 14.3$. Normally, the chopping current of VCB is set as 3–8 A [22].

2.2.2. Dielectric Strength

When the VCB is switching to open, the dielectric strength between the contacts increases with the increase of the distance between the contacts. When the transient recovery voltage between the contacts exceeds the dielectric strength, the gap between the contacts will break down and reignite. There is an approximately linear relationship between the dielectric strength U_b and the break time during reigniting, as described in the following [23]:

$$U_b = A(t - t_{open}) + B, \quad (2)$$

where A is the rate of dielectric strength rise (kV/s); B is dielectric strength constant of VCB at the moment of contact separation (kV); t is simulation time (s); and t_{open} is breaker opening time (s).

2.2.3. HF Arc Quenching Capability

When the HF current generated by the VCB reignition is close to zero, the VCB can extinguish it. Such an arc quenching capability can be described as the rate di/dt of the time change when the HF current is crossing zero. The HF current starts with a high rate of change that the VCB cannot turn off. However, with the attenuation of HF current, when the di/dt is less than a critical value when the current is crossing zero, the VCB will cut off HF current and turn it into a disconnected state, which is generally between 100–600 A/ μ s [24].

2.2.4. Arcing Voltage

In practice, the arc between contacts of the VCB will generate a voltage drop, and the arcing voltage is approximately 20 V [25]. A constant arcing voltage of 20 V is achieved by changing the value of controllable resistance in the customized model, as shown below [26]:

$$R_{arc} = \frac{u_{arc}}{i_{arc}}, \tag{3}$$

where R_{arc} is arcing resistance (Ω); u_{arc} is arcing voltage (V); and i_{arc} is arcing current (A).

The VCB in the simulation is equivalent to the controlled resistance R with the parallel branch, as shown in Figure 2, where $R_s = 50 \Omega$, $L_s = 50 \text{ mH}$, $C_s = 200 \text{ pF}$ [27]. The switching process of VCB is divided into four states in [21]. States 1–4 respectively represent the state before power frequency cut-off, transient voltage recovery, reignition, and complete switch-off. By measuring the VCB current i and the voltage u between two contacts, the C language is used to programming and solve the VCB chopping current I_{ch} , dielectric strength U_b , HF arc quenching ability, and arcing voltage u_{arc} . The program flow chart is shown in Figure 3. At the time t_{ch} when the chopping current occurring is more than 5 ms after the time t_{open} when the VCB starts operating, it can be considered that the VCB has been completely opened and there will be no reignition. The controllable resistance is realized as a real-time control by calling the program in PSCAD. Initially, the closed VCB is in State 1 and $R = 0$. Arcing occurs when the VCB starts to separate, and the program adjusts the controllable resistor R according to Equation (5) to maintain the voltage across the contacts as arcing voltage. When i is less than I_{ch} , the VCB enters State 2 after the first interruption, and $R = 1 \text{ M}\Omega$. When VCB is in State 2, if the transient voltage exceeds the dielectric strength, the VCB reignites and enters State 3, and the voltage across the contacts is the arcing voltage. When the VCB is in State 3, if the HF current quenching condition is satisfied, the current is cut off and the VCB returns to State 2, $R = 1 \text{ M}\Omega$. After multiple reignitions occur, when the transient recovery voltage cannot reach the dielectric strength, the VCB is successfully opened and remains in $R = 1 \text{ M}\Omega$.

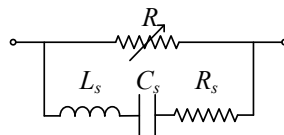


Figure 2. The vacuum circuit breaker (VCB) model.

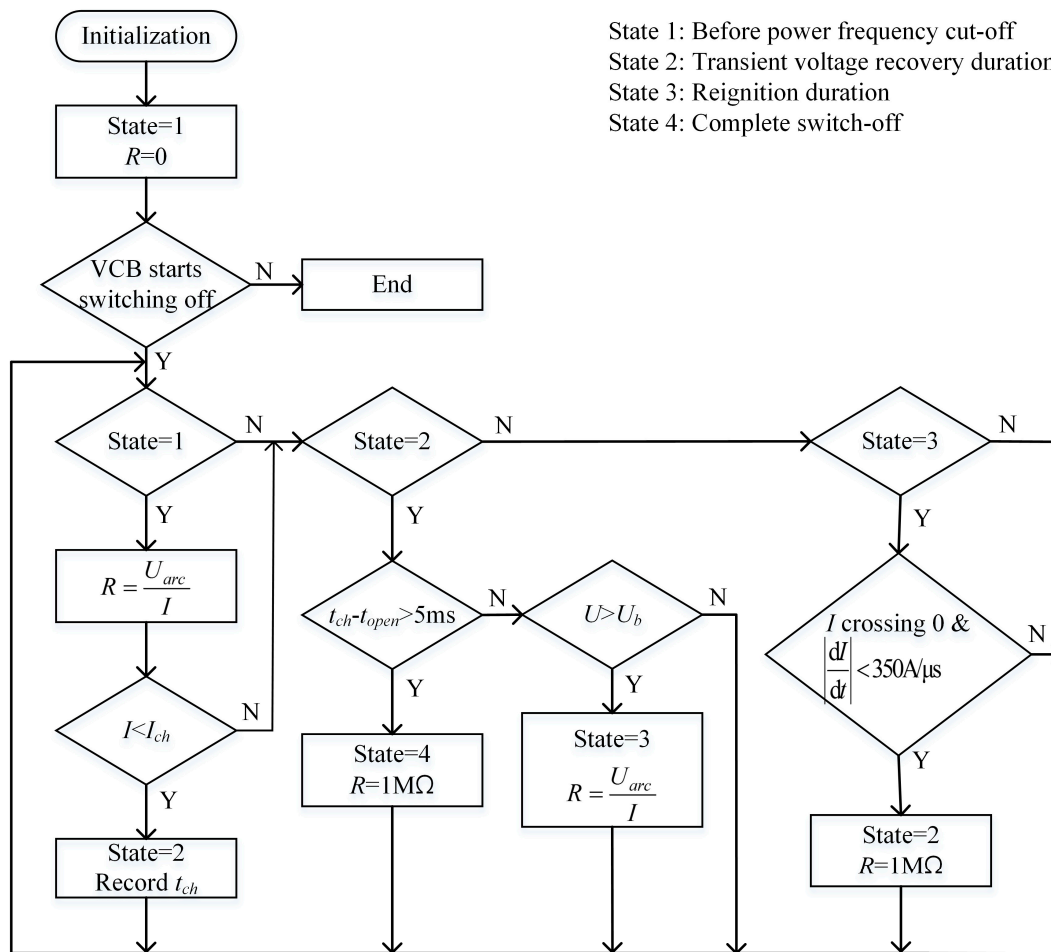


Figure 3. Block diagram of the VCB model.

2.3. Other Models

2.3.1. Transformer Model

In this paper, the unified magnetic equivalent circuit (UMEC) model is adopted for transformers, which can represent the phase coupling of the transformer in PSCAD. At the same time, capacitors are connected in parallel between the high-voltage side, low-voltage side, and high and low voltage of the transformer to simulate the HF characteristics of the transformer [28].

2.3.2. Submarine Cable Model

The frequency dependent (phase) model in PSCAD is used to model submarine cables. The three-core cable structure is used in the simulation, and the specific setting parameters are shown in [28].

3. Description of Experimental Test System and Model Verification

3.1. Description of Experimental Test System

The wiring diagram of the test system is shown in Figure 4. A transformer TX₁ with a transformation ratio of 10 kV/35 kV and a capacity of 10 MVA is used to simulate the main transformer of the offshore booster station and provides a 35 kV power supply. One kilometer-long and 80 m-long submarine cables, named Cable₁ and Cable₂ with a cross-section of 35 mm², are respectively connected to both sides of a 40.5 kV VCB to simulate the three-core MV cable between the 35 kV busbar to the

wind turbine at the beginning of the feeder and the transformer at the top of the tower to the VCB at the tower bottom. The technical characteristics of the VCB are shown in Table 1. A transformer TX₂ with a transformation ratio of 35 kV/ 0.69 kV and a capacity of 2 MVA simulates the terminal transformer of the wind turbine. A reactor with a capacity of 1.6 Mvar is set as the load, and its capacity is approximately 80% of TX₂ to ensure that the amplitude value of power frequency current flowing through the VCB is greater than the chopping current.

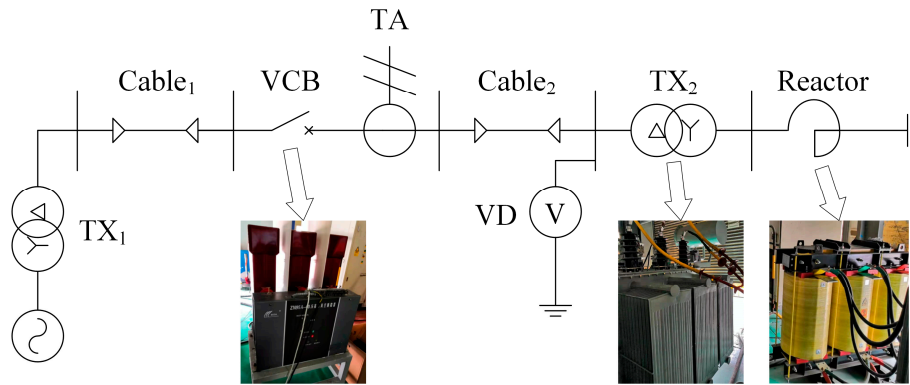


Figure 4. Wiring diagram of the test system

Table 1. Technical characteristics of the VCB.

Product Model	Rated Voltage (kV)	Rated Current (A)	Rated Short-Circuit Breaking Current (kA)	Average Opening Speed (m/s)	Clearance between Open Contacts (mm)
ZN95A-40.5	40.5	630	25	1.7	18

In order to measure and record HF signals, a 150 kV high-voltage probe VD with a ratio of 10000:1, of which the model is NRV-150, is used in the experiment. It has an accuracy of 1% when the frequency of voltage ranges from 10 Hz to 1 MHz. The model of HF current transformer TA is Pearson D101, with a frequency bandwidth of 0.25 Hz–4 MHz and 50 kA peak current. During the experiment, the sampling rate of the digital oscilloscope is set as 40 Msa/s.

3.2. Model Verification

When chopping current occurs in the VCB, the magnetic energy stored in the inductive load (such as reactor, no-load transformer, or motor, etc.) is converted into the electric field energy of the load side capacitance (usually the capacitance of the submarine cable), and thus overvoltage is generated. Therefore, the chopping current value can be calculated by the amplitude U_{max} of the first overvoltage generated by the chopping current:

$$U_{max} = \sqrt{(U_0 + U_n)^2 + (I_{ch} \cdot \sqrt{\frac{L_t}{C_t}})^2}, \tag{4}$$

where U_0 is cut-off transient voltage (V); U_n is power supply voltage (V); L_t is system equivalent inductance (H); and C_t is load side capacitance (F).

The reignition of the VCB is obvious when the inductive load is switched to separate. Therefore, the switching test is conducted under the condition of the inductive load to measure the three-phase voltage at the high-voltage side of TX₂ and the B-phase current at the outlet side of the VCB. The waveform obtained from the experiment is shown in Figure 5a.

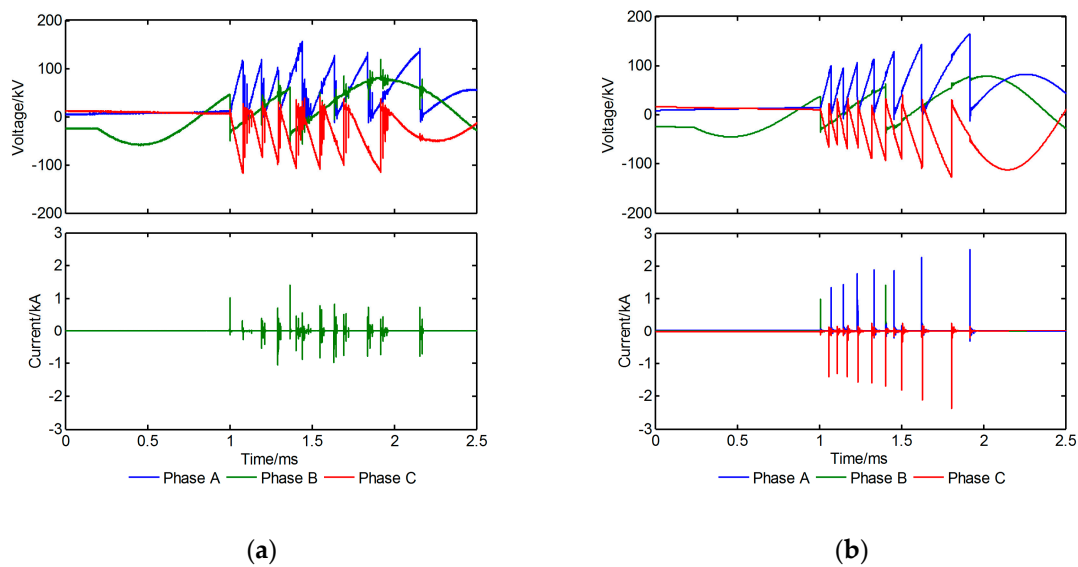


Figure 5. Voltage and current waveforms of experiment and simulation: (a) Waveforms of experiment voltage and current; (b) waveforms of simulation voltage and current.

According to Equation (4) and Figure 5a, the chopping current of VCB calculated in this experiment is 3.6 A. In Figure 5a, the value of the breakdown voltage is considered to be the value of the dielectric strength at this time. After the contacts of VCB begin to separate, each time a reignition occurs, the value of the breakdown voltage and the corresponding time are recorded and linearly fitted according to Equation (2), as shown in Figure 6. The relationship between dielectric strength and time is obtained as follows:

$$U_b = 7.355 \cdot 10^4 \cdot (t - t_{open}) + 0.69 \text{ kV}. \tag{5}$$

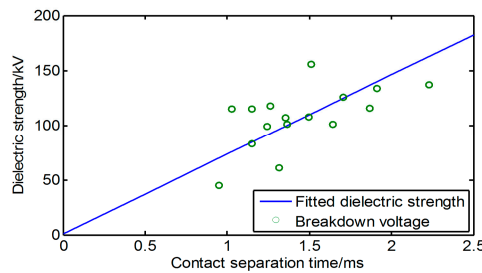


Figure 6. Dielectric strength versus contact separation time.

Since the HF arc quenching ability has little influence on the overvoltage, the critical value of di/dt is set as the average value of $350 \text{ A}/\mu\text{s}$ in this paper [29], and the arcing voltage is set as 20 V. The PSCAD 4.6.2 is used to simulate and model the experimental system shown in Figure 4. The reignition model introduced in Section 2.2 of this paper is adopted in the VCB model. By cooperating with the time logic device, the switching operation is realized at any time in the model, and the waveform is obtained by simulation, shown in Figure 5b.

In the case of switching off inductive load, because of the chopping current, the rising rate of transient recovery voltage between two contacts of VCB is much faster than that of dielectric strength, which causes a lot of restrikes of VCB, as shown in Figure 5a, where B-phase is the first-opening phase. In Figure 5a,b, the amplitude and the total number of reignition of B-phase overvoltage are basically the same, and the amplitude of HF current is basically the same. However, due to the interference of external factors on the measuring equipment in the actual experiment, the measured HF current has many burrs, but its amplitude is relatively small compared with HF current generated

by reignition. There is no burr in the simulation due to no external interference. As a result, the effectiveness of the VCB reignition model is well verified by the waveform of the switching TOV obtained in the experiment.

4. VCB Switching Modes of OWF Internal Electrical System

The switching modes of VCB inside the electrical system of OWF include normal switching and fault switching.

Normal switching: In this case, the no-load terminal transformer at the top of the tower is cut off; that is, after a certain wind turbine is out of operation, a corresponding VCB at tower bottom is switched off. Meanwhile, the rest wind turbines on the feeder remain in full load operation.

Fault switching: In this situation, the switching happens when wind turbines are in normal operation. Specifically, it includes two kinds of circumstances. One is that when the wind turbines are in full load operation on the whole feeder, the VCB at the beginning of the feeder is switched off. The second is that when the wind turbines are in full load operation on the whole feeder, a VCB at tower bottom is switched off.

5. Simulation of Internal Electrical System in OWF

5.1. Simulation System Setting

Wailuo OWF is located in Guangdong Province, China. Its installed capacity is 300 MW. In this section, Wailuo OWF is taken as an example to carry out simulation research. A calculation model of the internal electrical system of the OWF will be established based on the VCB and DFIG model mentioned above, as shown in Figure 7. The capacity of transformer T_0 is 180 MVA, with its ratio and leakage inductance of 220 kV/35 kV and 0.06, respectively. For transformer T_n ($n = 1, 2, \dots, 8$), the capacity is 5 MVA, the ratio is 35 kV/0.69 kV, and the leakage inductance is 0.02 per unit. The external grid, which is connected to T_0 with a 20-km-long submarine cable, is represented by a 220 kV ideal voltage source. The length of L_1 is 80 m, and the wind turbine (WT) connects to the transformer directly. The length of L_2 between each wind turbine is 640 m, and L_0 is 5 km long. The cross-section area of submarine cables is 300 mm². The three dielectric strength parameters of high-, medium-, and low-voltage have been proposed in [23] and have been used in many similar simulation studies. In this paper, the dielectric strength of "high voltage VCB", which is commonly used, is compared with the parameters obtained by experiments. In the simulation, the influence of two-parameter settings on overvoltage amplitude and steepness with normal switching and fault switching is compared. The parameters used are shown in Table 2.

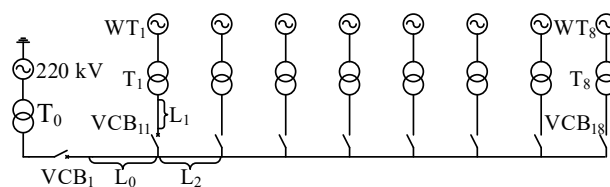


Figure 7. Wiring diagram of the simulation system.

Table 2. Traditional parameters and experimental parameters.

Parameters Type	A(kV/s)	B(kV)
traditional parameters	1.7×10^4	3.4
experimental parameters	7.355×10^4	0.69

Snapshots were taken after the stable operation of the system for 2 s, and each snapshot was started up and running for 0.08 s, with the simulation step length of 0.4 μ s. In order to reduce the

simulation time, a calculation model of the internal electrical system of OWF with eight DFIGs on a single feeder was built in this paper; the rated capacity of each DFIG is 4 MW. In the case of normal switching, the VCB is set to be switched off at the time of A-phase voltage zero-crossing. In the situation of fault switching, the VCB is set to be switched off at the time when A-phase current reaches the chopping current [30].

5.2. Relation Between Transformer Position and Overvoltage in Normal Switching

According to the circuit theory, when reignition occurs in the VCB, the TOV steepness on the high-voltage side of the terminal transformer is related to the current flowing through the capacitance of the high-voltage to the ground of the transformer, as shown in Equation (6):

$$\frac{du_T}{dt} = -\frac{i_T}{C_H}, \tag{6}$$

where u_T is the voltage at the high-voltage side of the terminal transformer (V); i_T is current in the capacitance of the high-voltage side to the ground of the terminal transformer (A); and C_H is the capacitance of the high-voltage to the ground of the transformer (F).

When any wind turbine on the feeder is out of operation, the terminal transformer and its 80 m connection cable are cut off. Then, the overvoltage on the high-voltage side of the terminal transformer on the feeder is measured, and the steepness is calculated. Since the rising rate of transient recovery voltage after switching is always lower than the rising rate of dielectric strength, they do not intersect, and there is no reignition. At this time, the amplitude and the steepness of the overvoltage at each position and the voltage waveform at the high-voltage side of transformer T₇ when switching off VCB₁₇ are respectively shown in Figures 8 and 9, in which overvoltage amplitude is per unit value as follows:

$$\sqrt{2} \cdot 35 \div \sqrt{3} = 28.58 \text{ kV}. \tag{7}$$

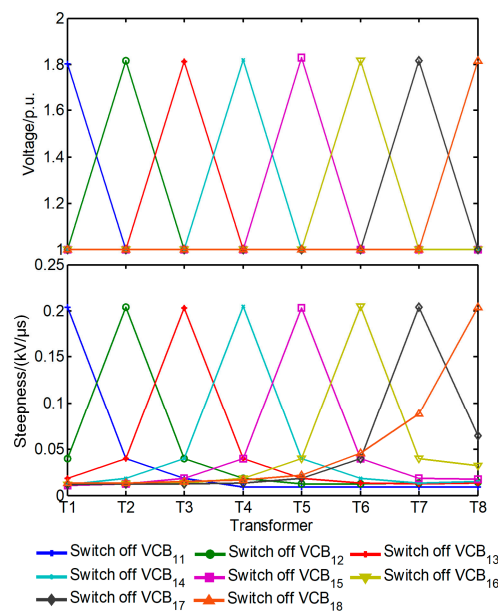


Figure 8. Overvoltage of transformers at different positions in the cases of switching off VCBs at the tower bottom normally using experimental parameters.

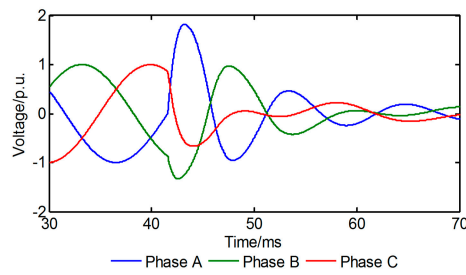


Figure 9. Overvoltage waveform of T_7 in the case of switching off VCB_{17} normally.

Figure 8 shows that the overvoltage amplitude and the maximum steepness of the transformer in the normal switching occur at the point where the VCB cuts out the transformer; they are 1.83 p.u. and 0.2 kV/ μ s, respectively. The overvoltage amplitude on the high-voltage side of the transformer of the other wind turbines in normal operation is basically 1 p.u., and the overvoltage steepness decreases with the increase of the propagation distance of the incident wave.

When the dielectric strength of VCB is simulated with traditional parameters, since the dielectric strength rises slowly, reignition occurs easily. The total reignition times in normal switching with different parameters are shown in Table 3. At this time, the total number of reignition normal switching is 10–14 times. The voltage amplitude and steepness of the high-voltage side of the terminal transformer at each position are shown in Figure 10. Compared with the results with experimental parameters, the maximum overvoltage amplitude drops from 1.83 p.u. to 1.58 p.u. However, the maximum overvoltage steepness reaches 76.7 kV/ μ s, increasing by about 380 times.

Table 3. Total reignition times in normal switching with different parameters.

Switching Case	Traditional Parameters	Experimental Parameters
normal switching	10-14	0

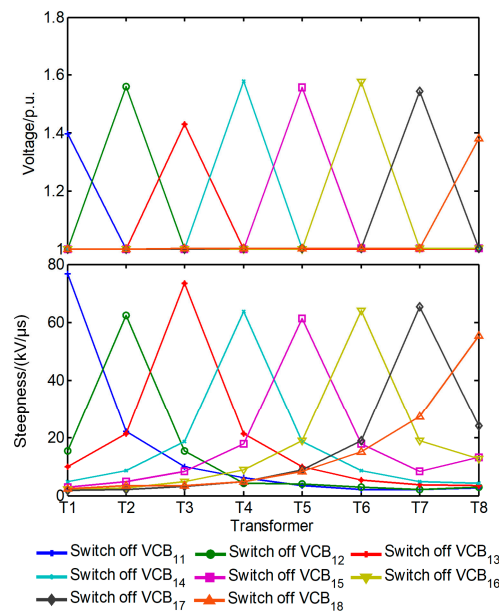


Figure 10. Overvoltage of transformers at different positions in the cases of switching off VCBs at the tower bottom normally using traditional parameters.

5.3. Relation between Transformer Position and Overvoltage in Fault Switching

5.3.1. VCB Switching at Feeder

When the wind turbines on the whole feeder line are in full-load operation, VCB₁ has no reignition in fault switching. The overvoltage waveform of the terminal transformer T₇ is shown in Figure 11. The overvoltage amplitude at the high-voltage side of the terminal transformer at all positions on the feeder is 1.27 p.u., and the maximum overvoltage steepness is about 0.1 kV/μs. When the traditional parameters are used in the simulation, VCB₁ will not have reignition. The simulation results of the two are consistent at this moment.

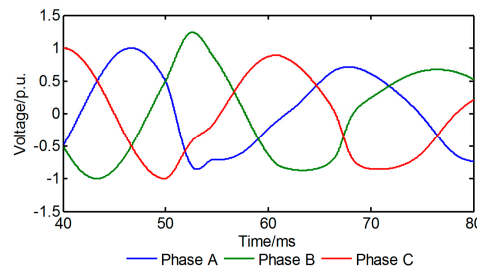


Figure 11. Overvoltage waveform of T₇ in the case of switching off VCB₁ faultily.

5.3.2. VCB Switching at Tower Bottom

When the wind turbines on the whole feeder are in full load operation, the VCB at the tower bottom has fault switching, and the simulation results are shown in Figure 12; it indicated that switching VCB only causes overvoltage with amplitude of about 1.18–1.42 p.u. on the high-voltage side of the terminal transformer where it is located, and the steepness is 83.3–142 kV/μs. The voltage amplitude of the remaining terminal transformer is 1 p.u. The voltage waveforms of terminal transform T₇ when VCB₁₇ switching and its adjacent terminal transformer T₈ at the high-voltage side are respectively shown in Figure 13a,b.

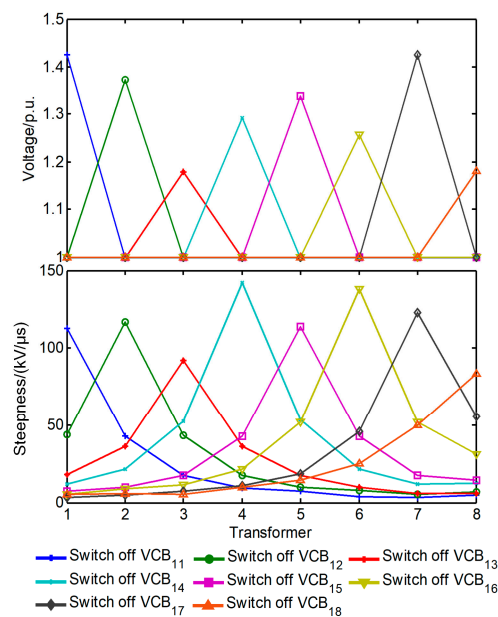


Figure 12. Overvoltage of transformers at different positions in the cases of switching off VCBs at the tower bottom faultily using experimental parameters.

During VCB₁₇ switching, an overvoltage with an amplitude up to 1.42 p.u. is generated due to reignition. After reaching the high-voltage side of T₈ through the 720 m cable, the overvoltage

amplitude rapidly attenuates, and the maximum steepness of voltage fluctuation also decreases from 123 kV/μs to 55.3 kV/μs. From Table 4, the total times of reignition in this condition is about 9–10.

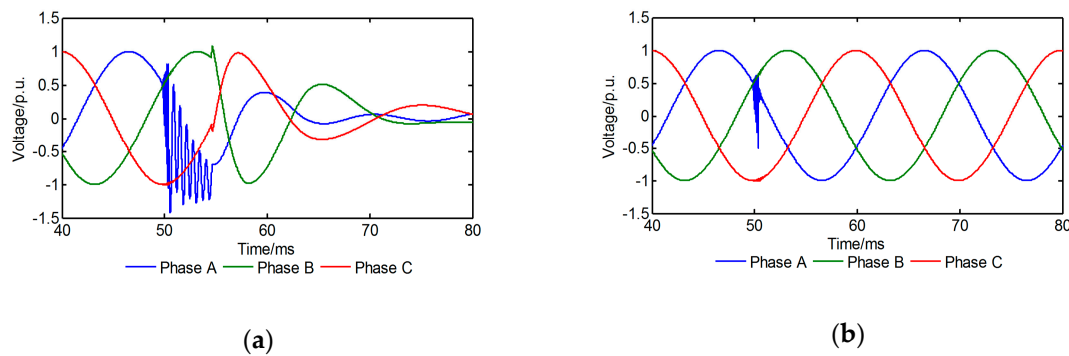


Figure 13. Voltage waveforms of T₇ and T₈ in the case of switching off VCB₁₇ faultily: (a) Voltage waveform of T₇; (b) voltage waveform of T₈.

Table 4. Total reignition times in fault switching with different parameters.

Switching Case		Traditional Parameters	Experimental Parameters
fault switching	at feeder	0	0
	at tower bottom	135–171	8–10

When traditional parameters are applied for simulation, the results are obtained shown in Figure 14. Due to the slow growth rate of dielectric strength, the numbers of reignition increase significantly to 135–171 times, and the maximum overvoltage amplitude increases from 1.42 p.u. to 2.96 p.u., which would cause the overvoltage amplitude of the terminal transformer at the high-voltage side of the adjacent wind turbine reaching 1.89 p.u.. Compared with the same condition when using experimental parameters, the amplitude of the switching terminal transformer increases about 2 times, and the overvoltage steepness increases about 1.5 times.

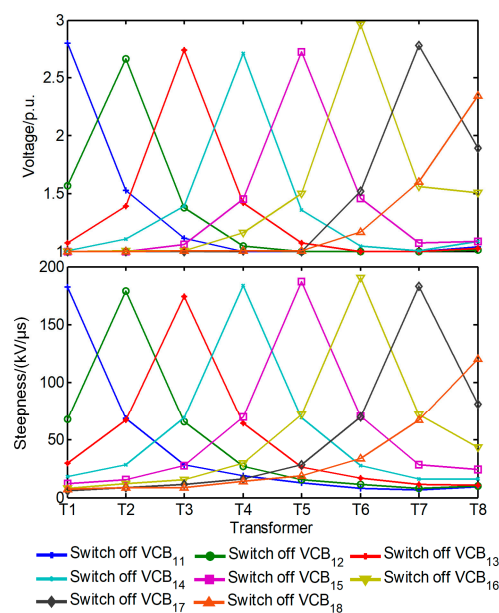


Figure 14. Overvoltage of transformers at different positions in the cases of switching off VCBs at the tower bottom faultily using traditional parameters.

6. Conclusions

In this paper, a test platform for a simplified MV cable collection system in OWF that can demonstrate the reignition phenomenon of VCB was constructed, and the parameters of VCB were calculated through experiments to verify the validity of the customized VCB model. A cable collection system of OWF was built according to the above model. The dielectric strength parameters of the VCB measured by the experiment were used in the simulation to study the TOV generated, and the results were compared with those of the traditional dielectric strength parameters. The following conclusions are drawn:

- (1) The overvoltage amplitude of the high voltage side of the transformer at different positions was basically the same in switching off feeder VCB. When the tower bottom VCB had normal or fault switching, the overvoltage steepness decreased with the increase of the propagation distance of the incident wave. The voltage amplitudes at the high-voltage side of the transformers in other positions were slightly influenced.
- (2) With experimental parameters, the critical overvoltage occurred in switching off VCBs at the tower bottom, the overvoltage amplitude in normal switching was the largest, up to 1.83 p.u., while the steepness of the overvoltage generated in fault switching was the largest, up to 142 kV/ μ s, and the total numbers of reignition were 9–10 times.
- (3) Due to the difference of dielectric strength of the VCB, when using the experimental parameters measured in this study, the amplitude of overvoltage of the terminal transformer was reduced to 1/2, and the steepness was reduced to 1/1.5 compared with using the traditional parameters of VCB under the same operation condition, in case of switching off VCB at the tower bottom with wind turbines full loading. Therefore, it is recommended that the actual experimental parameters of VCBs should be adopted in the following researches.

Author Contributions: Conceptualization, Z.Z. and Y.G.; methodology, X.J.; software, Z.Z. and Y.G.; validation, Y.G., X.J., and G.L.; investigation, H.D.; writing—original draft preparation, Z.Z.; writing—review and editing, Y.G. and X.J.; resources, M.Z.; visualization, X.L.; supervision, G.L.; project administration, W.T.

Funding: This research was funded in part by National Natural Science Foundation of China, grant number 51677073 and 51477054, in part by National Natural Science Fund & China-State Grid Joint Fund for Smart Grid, grant number U1766213.

Acknowledgments: The authors would like to thank Xinyu Jiang from Guangzhou Zhiguang Electric Co., Ltd. for his support on experiments.

Conflicts of Interest: The authors declare no conflict of interest.

References

1. Esteban, M.D.; Espada, J.M.; Ortega, J.M.; López-Gutiérrez, J.-S.; Negro, V. What about Marine Renewable Energies in Spain? *J. Mar. Sci. Eng.* **2019**, *7*, 249. [[CrossRef](#)]
2. Onea, F.; Rusu, L. A Study on the Wind Energy Potential in the Romanian Coastal Environment. *J. Mar. Sci. Eng.* **2019**, *7*, 142. [[CrossRef](#)]
3. Gintautas, T.; Sørensen, J.D. Improved Methodology of Weather Window Prediction for Offshore Operations Based on Probabilities of Operation Failure. *J. Mar. Sci. Eng.* **2017**, *5*, 20. [[CrossRef](#)]
4. Lei, Y.; Jian, W.; Gang, L.; Hui, M.; Ming, Z. Thermal Rating of Offshore Wind Farm Cables Installed in Ventilated J-Tubes. *Energies* **2018**, *11*, 545.
5. Wang, P.Y.; Ma, H.; Liu, G.; Han, Z.Z.; Kang, L.Y. Dynamic Thermal Analysis of High-voltage Power Cable Insulation for Cable Dynamic Thermal Rating. *IEEE Access* **2019**, *7*, 56095–56106. [[CrossRef](#)]
6. Wang, P.; Liu, G.; Ma, H.; Liu, Y.; Xu, T. Investigation of the Ampacity of a Prefabricated Straight-Through Joint of High Voltage Cable. *Energies* **2017**, *10*, 2050. [[CrossRef](#)]
7. Xie, Y.; Liu, G.; Zhao, Y.; Li, L.; Ohki, Y. Rejuvenation of retired power cables by heat treatment. *IEEE Trans. Dielectr. Electr. Insul.* **2019**, *26*, 668–670. [[CrossRef](#)]
8. Xie, Y.; Zhao, Y.; Liu, G.; Huang, J.; Li, L. Annealing Effects on XLPE Insulation of Retired High-Voltage Cable. *IEEE Access* **2019**, *7*, 104344–104353. [[CrossRef](#)]

9. Sweet, W. Danish wind turbines take unfortunate turn. *IEEE Spectr.* **2004**, *41*, 30. [[CrossRef](#)]
10. Zhou, J.; Xin, Y.; Tang, W.; Liu, G.; Wu, Q. Impact Factor Identification for Switching Overvoltage in an Offshore Wind Farm by Analyzing Multiple Ignition Transients. *IEEE Access* **2019**, *7*, 64651–64662. [[CrossRef](#)]
11. Shipp, D.D.; Dionise, T.J.; Lorch, V.; Macfarlane, B.G. Transformer failure due to circuit breaker induced switching transients. *IEEE Trans. Ind. Appl.* **2011**, *47*, 707–718. [[CrossRef](#)]
12. Xin, Y.; Tang, W.; Zhou, J.; Yang, Y.; Liu, G. Sensitivity analysis of reignition overvoltage for vacuum circuit breaker in offshore wind farm using experiment-based modeling. *Electr. Power Syst. Res.* **2019**, *172*, 86. [[CrossRef](#)]
13. Villar, F.S.; Reza, M.; Srivastava, K.; Silva, L. High frequency transients propagation and the multiple reflections effect in collection grids for offshore wind parks. In Proceedings of the Power & Energy Society General Meeting, Detroit, MI, USA, 24–28 July 2011; pp. 1–7.
14. Liljestr and, L.; Sannino, A.; Breder, H.; Thorburn, S. Transients in collection grids of large offshore wind parks. *Wind Energy* **2008**, *11*, 45–61. [[CrossRef](#)]
15. Wang, X.; Liu, X.; Li, Y.; Saboor, A.; Cao, J.; Shang, Y. Study on switching transients of cable collector system in wind power plant. In Proceedings of the 2011 1st International Conference on Electric Power Equipment-Switching Technology, Xi'an, China, 23–27 October 2011; pp. 308–311.
16. Ghafourian, S.; Arana, I.; Holboll, J.; Sorensen, T.; Popov, M.; Terzija, V. General Analysis of Vacuum Circuit Breaker Switching Overvoltages in Offshore Wind Farms. *IEEE Trans. Power Deliv.* **2016**, *31*, 2351–2359. [[CrossRef](#)]
17. Glasdam, J.; Bak, C.L.; Hjerrild, J. Transient studies in large offshore wind farms employing detailed circuit breaker representation. *Energies* **2012**, *5*, 2214–2231. [[CrossRef](#)]
18. Holdsworth, L.; Wu, X.G.; Jenkins, N.; Ekanayake, J.B. Dynamic modeling of doubly fed induction generator wind turbines. *IEEE Trans. Power Syst.* **2003**, *18*, 803–809.
19. Xu, B.; Zhang, Z.; Li, C.; Zhan, P.; Wen, J. LCL filters applied in doubly fed induction generator. *Electric Power Autom. Equip.* **2015**, *35*, 44–50.
20. Badrzadeh, B.; Hogdahl, M.; Isabegovic, E. Transients in Wind Power Plants—Part I: Modeling Methodology and Validation. *IEEE Trans. Ind. Appl.* **2012**, *48*, 794–807. [[CrossRef](#)]
21. Ghafourian, S.M. Switching Transients in Large Offshore Wind Farms. Ph.D. Thesis, The University of Manchester, Manchester, UK, 2015.
22. Abdulahovic, T.; Thiringer, T.; Reza, M.; Breder, H. Vacuum Circuit Breaker Parameter Calculation and Modelling for Power System Transient Studies. *IEEE Trans. Power Deliv.* **2017**, *32*, 1165–1172. [[CrossRef](#)]
23. Glinkowski, M.T.; Gutierrez, M.R.; Braun, D. Voltage escalation and reignition behavior of vacuum generator circuit breakers during load shedding. *IEEE Trans. Power Deliv.* **1997**, *12*, 219–226. [[CrossRef](#)]
24. Xin, Y.; Bo, L.; Tang, W.; Wu, Q. Modeling and Mitigation for High Frequency Switching Transients Due to Energization in Offshore Wind Farms. *Energies* **2016**, *9*, 1044. [[CrossRef](#)]
25. Leusenkamp, M.B.J. Vacuum interrupter model based on breaking tests. *IEEE Trans. Plasma Sci.* **1999**, *27*, 969–976. [[CrossRef](#)]
26. Popov, M. Switching three-phase distribution transformers with a vacuum circuit breaker: Analysis of overvoltages and the protection of the equipment. Ph.D. Thesis, Delft University of Technology, Delft, The Netherlands, 2002.
27. Helmer, J.; Lindmayer, M. Mathematical modeling of the high frequency behavior of vacuum interrupters and comparison with measured transients in power systems. In Proceedings of the 17th International Symposium on Discharges and Electrical Insulation in Vacuum, Berkeley, CA, USA, 21–26 July 1996; pp. 323–331.
28. Liu, G.; Guo, Y.; Xin, Y.; Lei, Y.; Tang, W. Analysis of switching transients during energization in large offshore wind farms. *Energies* **2018**, *11*, 470. [[CrossRef](#)]
29. Abdulahovic, T. Analysis of High-Frequency Electrical Transients in Offshore Wind Parks. Ph.D. Thesis, Chalmers University of Technology, Gothenburg, Sweden, 2011.
30. Reza, M.; Breder, H. Cable System Transient Study: Vindforsk V-110: Experiments with Switching Transients and Their Mitigation in a Windpower Collection Grid Scale Model. Available online: <https://energiforskmedia.blob.core.windows.net/media/19748/cable-system-transient-study-elforskrappport-2009-05.pdf> (accessed on 30 September 2019).



© 2019 by the authors. Licensee MDPI, Basel, Switzerland. This article is an open access article distributed under the terms and conditions of the Creative Commons Attribution (CC BY) license (<http://creativecommons.org/licenses/by/4.0/>).